MOLEKUL
eISSN: 2503-0310

Articles
https://doi.org/10.20884/1.jm.2023.18.1.7077

Does Divacancy Defect Combine with N,S-Codoping Enhance the Electronic Properties of Graphene to Its Interaction with K^+ Ion?

Yuniawan Hidayat*, Fitria Rahmawati, Khoirina D Nugrahaningtyas, Abduro'uf Althof Abiyyi

Chemistry Department, Sebelas Maret University, Jl. Ir Sutami 36A Surakarta, Indonesia

*Corresponding author email: yuniawan.hidayat@staff.uns.ac.id

Received November 03, 2022; **Accepted** February 15, 2023; **Available online** March 20, 2023

ABSTRACT. Defects in graphene alter its structure, electrical characteristics, and interaction with K^+ ions. The related characteristics of divacancy defect graphene and N, S codoped divacancy graphene were effectively explored using the DFTB technique. Divacancy is essential for the band gap opening. The dopants considerably enhance the density of state (DOS) intensity and alter the graphene-character bands. The depletion of density caused by the dopant is seen on the charge density isosurface. Because the charge of the K^+ ion is balanced by the dopant, the ion prefers to be adsorbed on divacancy graphene with dopants.

Keywords: divacancy graphene, DFTB, fermi level, K^+ adsorption, N,S-codoping

INTRODUCTION

The electrical potential of the graphene anode in a potassium ion battery may be tuned to maximize the interaction with the K^+ ions (Hidayat et al., 2022). Nitrogen-doped graphene has unique properties compared to pristine graphene. The charge density of carbon's surface is affected by the dopant and acts as an active site as a catalyst. Furthermore, the dopant responsible for the fermi level shifted above the Dirac point and pressed the DOS near Fermi to produce the gap between the conduction and valency bands (Joucken et al., 2015; Ketabi et al., 2016).

The mechanical, thermal, and electrical conductivities properties of a crystal are all affected by defects in the crystal. A vacancy defect in graphene was caused by the loss of one or more carbon atoms, resulting in deformation in the bond length around the defect point (Olsson et al., 2019). On the surface of graphene, vacancy defects influence electron transfer, lowering graphene's conductivity but enhancing ion diffusivity and chemical reactivity (Pašti et al., 2018). Metal adsorption in the vacancy of graphene is energetically more favorable than on pristine graphene (Olsson et al., 2019). Dopants such as Nitrogen (N), Sulphur (S), Boron (B), and Phosphorus (P) can be advanced the electronic properties of graphene (Li et al., 2016). The simultaneous employment of two distinct dopants leads to a combination effect such as potential parameter, current density, and increased electron transport (Rivera et al., 2017; Su et al., 2013; Z. Yang et al., 2013; Zhu et al., 2013). The combination of vacancy defect and doped graphene advantage enhances the performance of carbon-based anode materials.

DFTB (Density Functional Tight Binding) is a method based on a semiempirical approach that has roughly the same accuracy as the DFT method but the calculation time is shorter. The benefit of the DFTB technique is that it makes it feasible to compute the electronic structural characteristics of large molecule systems, which cannot be taken advantage of by the conventional ab initio method (Spiegelman et al., 2020). The DFTB approach has been effectively applied to examine redox reaction systems and anticipates features of molecular electronics related to the chemical activity of solids, supramolecules, and carbon (Poh et al., 2016; Selli et al., 2017; Sengupta et al., 2021; Zhang et al., 2020).

This work presents the DFTB approach for investigating the relationship of vacancy defect graphene with the presence of co-dopant N and S to its electronic behavior in terms of fermi level shifts, DOS changes, and energy band structures. Their impact on interactions with the K^+ ion was also studied. To clarify, four graphene structural models were used: divacancy graphene (V_2G), N, S codoped divacancy graphene (NSV_2G), K^+ ion on divacancy graphene ($K\text{-}V_2G$), and K^+ ion on the N and S doped divacancy graphene ($K\text{-}NSV_2G$).

EXPERIMENTAL SECTION

Pristine graphene based on the crystal characteristics of Kristin Person, 2014 (Persson, 2014) was modified to divacancy graphene (V_2G)

and N and S-doped divacancy graphene (NSV_2G). The lengths of the lattice lines a, b, and c are 2.468, 2.468, and 8.685, respectively, whereas the lattice angle of $\alpha = \beta$ is 90° and the angle of γ is 120°. The C atom's lattice coordinates are 0, 0, ¾; 0, 0, ¼; ⅓, ⅔, ¾; and ⅔, ⅓, ¼. The crystal follows a hexagonal structure with a point group of 6/mmm. A new unit cell PG with the dimensions 4x4x1 is generated with those parameters Using VESTA (Visualization for Electronic and Structural Analysis)(Momma et al., 2008). The V_2G was created by removing two adjacent carbon atoms of pristine graphene structure. The NSV_2G structure was created by substituting two C atoms with N and S atoms, in the VG structure. The N atom that replaces the C atom is located on the side of the hole to form a pyridinic structure. The K-V_2G and K-NSV_2G were modeled by putting the K^+ -ion in the center of the graphene's vacancy.

For calculation sampling, the unit cell was transformed into a supercell of 40 x 40 x1 and then optimized. The SCC (self-consistent charges)-DFTB approach was utilized for optimization, with the p-orbital defined as the maximal angular momentum for each atom. The Slater-Koster parameter 3ob-3-1 was used. The Hubbard Derivs was employed for each element. The fermi occupancy method was used to address the orbitals. Brillouin zone K-points were set up as Γ (0.0 0.0 0.0), M (0.5 0.0 0.0), and K (0.3333 0.333 0.0). The calculation was performed by the DFTB+ software(Hourahine et al., 2020)

The optimized-state calculation generated the density of state (DOS), fermi level, atomic charges, and band energy structure of each model. The DOS graphic and band structure were then tuned to Fermi level = 0, which was determined by E_o - E_f. The E_o is the Fermi level of 0 eV and E_f is the calculated-Fermi level. The energy formation of the defect graphene was calculated by equation 1

$$E_f = (E_{sys} - n_d E_d + n_c E_c - E_{pris}) \quad (1)$$

The total energy of graphene with vacancy, doping, or both is referred to as the E_{sys}. The E_{pris} represented the whole energy of pristine graphene. The energy of doped and removed carbon atoms in graphene, respectively, was denoted as E_d and E_c. The numbers n_d and n_c stand for the dopants and the removed carbons, respectively. Using N_2 and S_2 as a reference, the E_d of N and S was estimated using the DFTB technique. The atomic energy was found by dividing the total energy by 2. The E_c of the removed C atom was determined using a similar approach, by dividing the total energy of the ideal graphene primitive unit cell by the number of carbons.

Interaction ion K^+ over the graphene surface in terms of the adsorption energy was calculated by the following equation 2.

$$E_{ads} = E_{complex} - (E_{graphene} + E_{ion}) \quad (2)$$

The Energy of complex structure is defined as the energy of defect graphene structure with K^+ ion, that is K-V_2G and K-NSV_2G. $E_{graphene}$ refers to the energy of defect graphene without ions, that is V_2G and NSV_2G. The last term, E_{ion} refers to the energy of the K^+ ion.

RESULTS AND DISCUSSION

The DFTB method has successfully optimized the geometry structures of the modeled graphene. All modeled graphene is depicted in **Figure 1**. Lattice vector α after optimization is 2.41 Å, 2.45 Å, 2. 49 Å and 2.48 Å for V_2G, NSV_2G, K-V_2G, and K-NSV_2G, respectively. This result is in good agreement with the experimental study, mostly analyzed using X-ray and neutron diffraction the lattice vector was reported as 2.43 Å and 2.5 Å for vacant defect and doped graphene, respectively (Krishna et al., 2017; Phillips et al., 2021; Sheka et al., 2015). The divacancy graphene loses the symmetry near the vacant site, and the two opposite C-C which were connected to the same C atoms before being removed has a shortened distance of 2.06 Å than in pristine graphene (~2.46 Å)(Yin et al., 2014). It is in accordance with the calculation results of Pulido et al. who found the shortest distance around the vacant site was 1.95 Å (Pulido et al., 2011). Substitution by replacing two atom C with N and S in the V_2G make the relaxation of the corresponding distance to be 2.56 Å for C-N and 2.27 Å for C-S (**Figure 1b**). The calculated C-S distance is 1.75 Å, which is consistent with the estimated computation of other DFT methods (Lu et al., 2017). In the meanwhile, the C-N bond distance is 1.37 Å. Adsorption of K^+ ion on the vacant site in both graphene is responsible for the increase of the corresponding distance, i.e. 2.15 Å for V_2G and 2.66 Å (C-N) and 2.59 (C-S) for NSV_2G (**Figure 1c** and **1d**).

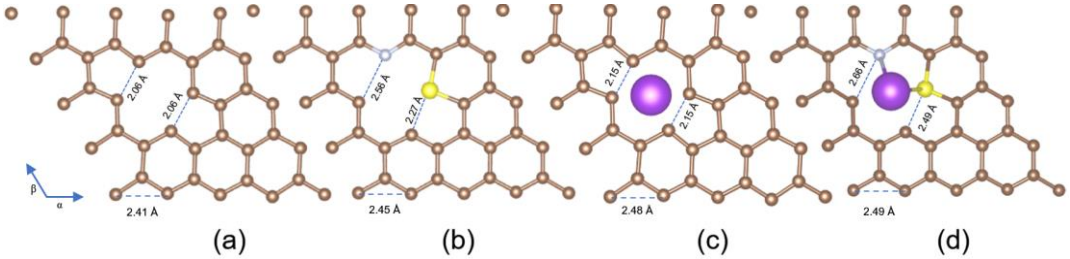

Figure 1. The optimized structure of (**a**) V_2G (**b**) NSV_2G (**c**) K-V_2G (**d**) K-NSV_2G. Brown refers to C, light blue refers to N, yellow refers to S and magenta refers to the K^+ ion

All the C-C distances of the graphene were statistically transformed into the normal distribution graph. **Figure 2** depicts the normal distribution of the C-C distance. The non-single bar in the graph confirms the variety of the C-C distance, indicating a symmetrical decreasing level of graphene by the vacant defect. The V_2G has 6 bars, which means that 6 types of C-C distances are observed, ranging between 1.370 to 1.470 Å (**Figure 2a**). The probability to find 1.41 Å of C-C distance is higher than others (23%), meeting with the average corresponding distance in the pristine graphene (Pulido et al., 2011; Wang et al., 2017; W. Zhang et al., 2020). It reveals that near the vacant site, the graphene loses its symmetry, and far from it, the symmetry remains. **Figure 2b** shows the average C-C distance of 1.43 Å with a probability of 27.5% for NSV_2G, indicating the average distance affected by the presence of N and S dopants. The adsorption of K^+ ion influences the C-C distance distribution; a new bar appears at 1.49 Å and the average distance turn to 1.40 Å. To accommodate the K^+ ion, the C-C distance around the vacancy is relaxed and the other is compressed (**Figure 2c**). The structural adjustment was also observed in NSV_2G during the K^+ ion adsorption. According to **Figure 1d**, the average C-C distance of 1.43 has a probability of 31%, which is higher than before ion adsorption. This was quickly followed by the disappearance of the bars at 1.38, 1.4, and 1.46 Å. This phenomenon confirms that the C-C distance is adjusted to compromise ion absorption compensation.

The defect energy formation of several types of graphene is shown in **Table 1**. The defect formation energy of the monovacancy was reported at the range 7.4 - 7.9 eV, while the presence of N dopant in the corresponding monovacancy graphene reduce the energy at the range 4.9 - 5.9 eV. The energy formation of divacancy graphene has a little bit higher than the monovacancy defect at a range of 7.7 - 8.8 eV. The corresponding energy of 7.9 eV is obtained from the DFTB method. Here, the optimized geometry of the graphene by the DFTB method is in good agreement with the DFT results. Divacancy graphene with N and S dopants has lower energy formation, following the previous trend of the monovacancy and the N dopant case. Defect formation including vacancy formation has been studied using Extreme ultraviolet irradiation (EUV) and UV light-sensitive. The formation of the vacancy defect was observed below 20 eV, moreover, at 8.3 eV the vacant site was initiated (Dong et al., 2022; Gao et al., 2014). Here, the DFTB results are in accordance with the experiment data.

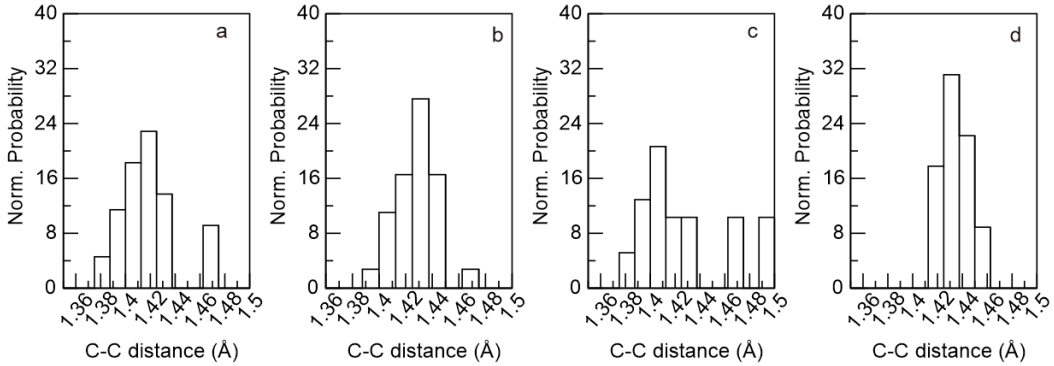

Figure 1. Normal probability of C-C distance distribution for (**a**) V_2G (**b**) NSV_2G (**c**) K-V_2G (**d**) K-NSV_2G

Table 1. The defect formation energy (E_f) of graphene with defect and dopant. V_1 = monovacancy, V_2 = divacancy, N = Nitrogen dopant, S = Sulfur dopant

Defect	Methods	E_f (eV)	Reff.
V_1	DFT	7.4-7.9	(Dai et al., 2011; Faccio et al., 2012; Rodrigo et al., 2016)
	DFTB	7.6-8.4	(Hidayat et al., 2022; Rodrigo et al., 2016)
NV_1	DFT	4.9-5.9	(Yang et al., 2015; Yu, 2013)
	DFTB	4.9	(Yu, 2013)
V_2	DFT	7.7-8.25	(Dai et al., 2011; Yu, 2013)
	Ab-initio	8.8	(El-Barbary et al., 2003)
Defect formation	EUV	Less than 20 eV	(Gao et al., 2014)
Defect Formation	UV light-sensitive	8.3 eV	(Dong et al., 2022)
	DFTB	7.91	This work
NSV_2	DFTB	7.10	This work

Electronic properties in terms of band structure and DOS of the graphene are depicted in **Figure 2**. The spectrum of both properties has been shifted to zero (E_0-E_f). The fermi level of the V_2G. As shown in Figure 2a, the opening band structure was observed for the V_2G and no electron intensity rises right at the $E_f = 0$ as shown by the DOS spectrum. However, width resonance occurred over the fermi level at 1.7 eV, indicating dispersionless of the π-character band. The scanning tunneling microscopy investigation by Miguel et al. observed the band opening for divacancy graphene. The DOS spectrum was also reported to have a V-shape with fluctuating intensity over the Fermi level (Ugeda et al., 2012). The gap between the conductance and valence band in NSV_2G is wider than in V_2G, but the presence of N and S dopants emerged a spectrum intensity between the band gap. It confirms by the DOS intensity at the fermi level (**Figure 2b**).

The bands represent the range of energy levels that electrons may have within them. Since the modeled graphene is 2D (planar), no direction to the z axes. At the K direction, the opening bands are observed along the Brillouin zone, which is contributed electronically by px and py. However, the DOS spectra come from the total DOS of s and p (p_x, p_y, and p_z) orbitals. The closed DOS spectra of the fermi region are affected by the p_z, where the electron remains with less affected by the vacant site (**Figures 2a** and **2b**). Performing DFT in a similar system, Coleman et al. showed clearly that partial DOS of the p_z is dominant at the fermi region with closed spectra, and no gap between valence and conductance band (Coleman et al., 2008).

As depicted in **Figure 2c**, the intensity in the conductance band structure of V_2G rises when the K^+ ion is adsorbed. The band gap at the Dirac point (K) remains the same. The DOS did not display any intensity at $E_f = 0$, but the spectrum does at Ef = 1.3 to 3.0. The K^+ ion charge affects the π-character bands of the V_2G. At the fermi region of K-NSV_2G, the band intensity at the fermi level is unraveled (**Figure 2d**). It was confirmed by the DOS spectrum intensity at $E_f = 0$ was lower than NSV_2G. The charge of the K^+ ion is distributed in the vacant site of graphene and the dopants.

The isosurface of total charge density (e/a_0^3) of the 2 x 2 x 1 graphene surface is depicted in Figure 3. As shown in **Figure 3a**, the charge density of the C-C bond in V_2G spread uniformly. These findings are in agreement with warner's paper (Warner et al., 2013). The depletion of the density is observed with the presence of the dopants in NSV_2G (**Figure 3b**). The N dopant dominantly withdraws the charge from the graphene surface. Adsorbing the K^+ ion, the graphene surface of the V_2G redistributes the charge to the atom carbon to balance the ion charge (Figure 3c) and degrades the charge density of the C-C bond. The C-C color turns to greenish yellow and the C atom turn red. In contrast to NSV_2G, the dopant balances the charge of the adsorbed K^+ ion, resulting in a thickening of the charge density of the C-C bond (**Figure 3d**).

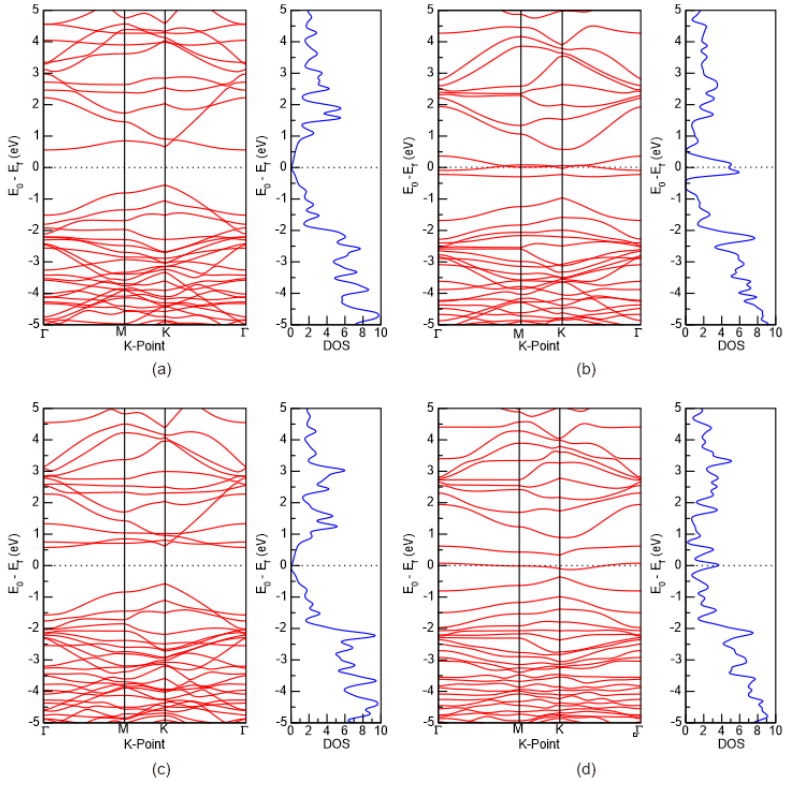

Figure 2. DOS and Electronic band structure of (**a**) V_2G (**b**) NSV_2G (**c**) K-V_2G (**d**) K-NSV_2G

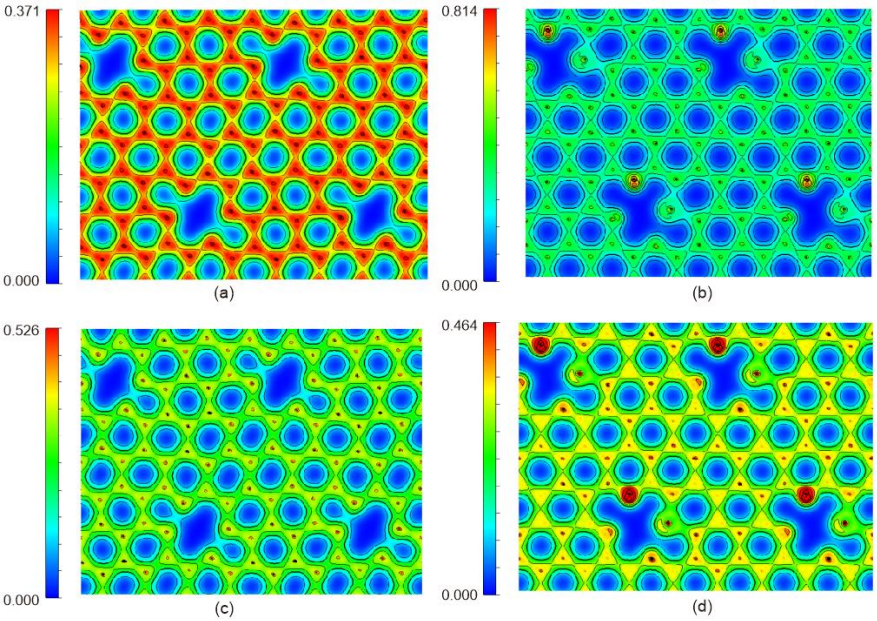

Figure 3. The total charge density of 2 x 2 x 1 graphene surface. (**a**) V_2G (**b**) NSV_2G (**c**) K-V_2G (**d**) K-NSV_2G.

Table 2. The partial charge and adsorption energy of K^+ ion in V_2G and NSV_2G and

Type	E_{ads}	K Charge
K-V_2G	-0.76 eV	0.83
K-NSV_2G	-2.38 eV	0.72

The adsorption energy of the K^+ ion on the V_2G and NSV_2G surfaces is presented in Table 2. The adsorption energy on the V_2G is -0.76 eV. It means that to separate the ion from graphene needs an energy of at least 0.76 eV. However, it is lower than on the monovacancy graphene (1,9 to 2.2 eV) (Hidayat et al., 2022; Pašti et al., 2018). The loss of two atoms C in the V_2G makes the K^+ ion in the vacant site easier to be released. The adsorption energy rises with the presence of N and S dopant to 2.38 eV, near to the adsorption energy of K^+ ion on S_2V_2G (2.32 eV) which was reported by Shanmugam, et al(Shanmugam et al., 2020). Meanwhile, the charge of the K^+ ion reduces to 0.83 and 0.72 on the V_2G and NSV_2G, respectively. It confirms that there is more electron transfer to the ion on the NSV_2G. The K^+ prefers interacts to the graphene with the dopant.

CONCLUSIONS

The DFTB approach successfully investigated the structure and electronic properties of divacancy graphene (V_2G) and the NS-doped divacancy graphene (NSV_2G). The variety of the C-C distance distribution reveals the unsymmetrical structure of the divacancy of graphene and the NS-divacancy graphene. Divacancy defect causing the band gap opening and the presence of the NS-dopants increase the electronic activity in the fermi region. The depletion of the charge density of graphene is affected by the electronic withdrawal of the dopant. Adsorbed K^+ ion affects the intensity of the DOS, changing the π-character bands of the graphene. The dopant and the adsorbed ion are responsible for the decrease of the charge density on the graphene surface. The K^+ ion prefers to be adsorbed on the divacancy graphene with dopants.

ACKNOWLEDGMENTS

This research was supported by Sebelas Maret University through Fundamental Research Grant.

REFERENCES

Coleman, V. A., Knut, R., Karis, O., Grennberg, H., Jansson, U., Quinlan, R., Holloway, B. C., Sanyal, B., & Eriksson, O. (2008). Defect formation in graphene nanosheets by acid treatment: An x-ray absorption spectroscopy and density functional theory study. *Journal of Physics D: Applied Physics*, *41*(6). https://doi.org/10.1088/0022-3727/41/6/062001

Dai, X. Q., Zhao, J. H., Xie, M. H., Tang, Y. N., Li, Y. H., & Zhao, B. (2011). First-principle study of magnetism induced by vacancies in graphene. *The European Physical Journal B*, *80*(3), 343–349. https://doi.org/10.1140/epjb/e2011-10955-x

Dong, G., Ding, S., & Peng, Y. (2022). Ultraviolet-Sensitive Properties of Graphene Nanofriction. *Nanomaterials*, *12*(24). https://doi.org/10.3390/nano12244462

El-Barbary, A. A., Telling, R. H., Ewels, C. P., Heggie, M. I., & Briddon, P. R. (2003). Structure and energetics of the vacancy in graphite. *Physical*

Review B, *68*(14), 144107. https://doi.org/10.1103/PhysRevB.68.144107

Faccio, R., & Mombrú, A. W. (2012). Magnetism in multivacancy graphene systems. *Journal of Physics: Condensed Matter*, *24*(37), 375304. https://doi.org/10.1088/0953-8984/24/ 37/ 375304

Gao, A., Lee, C. J., & Bijkerk, F. (2014). Graphene defect formation by extreme ultraviolet generated photoelectrons. *Journal of Applied Physics*, *116*(5), 054312. https://doi.org/10.1063/1.4892485

Hidayat, Y., Rahmawati, F., Nugrahaningtyas, K. D., Althof Abiyyi, A., Erlangga, M. Z., & Pujiastuti, N. (2022). Exploring the electronic properties of N-doped graphene on graphitic and pyridinic models and its interaction with K. *Australian Journal of Chemistry*, *75*(5), 325–330. https://doi.org/10.1071/CH21264

Hourahine, B., Aradi, B., Blum, V., Bonafé, F., Buccheri, A., Camacho, C., Cevallos, C., Deshaye, M. Y., Dumitrică, T., Dominguez, A., Ehlert, S., Elstner, M., van der Heide, T., Hermann, J., Irle, S., Kranz, J. J., Köhler, C., Kowalczyk, T., Kubař, T., Lee, I. S., Lutsker, V., Maurer, R. J., Min, S. K., Mitchell, I., Negre, C., Niehaus, T. A., Niklasson, A. M. N., Page, A. J., Pecchia, A., Penazzi, G., Persson, M. P., Řezáč, J., Sánchez, C. G., Sternberg, M., Stöhr, M., Stuckenberg, F., Tkatchenko, A., Yu, V. W. -z., & Frauenheim, T. (2020). DFTB+, a software package for efficient approximate density functional theory based atomistic simulations. *The Journal of Chemical Physics*, *152*(12), 124101. https://doi.org/10.1063/1.5143190

Joucken, F., Tison, Y., Le Fèvre, P., Tejeda, A., Taleb-Ibrahimi, A., Conrad, E., Repain, V., Chacon, C., Bellec, A., Girard, Y., Rousset, S., Ghijsen, J., Sporken, R., Amara, H., Ducastelle, F., & Lagoute, J. (2015). Charge transfer and electronic doping in nitrogen-doped graphene. *Scientific Reports*, *5*(1), 14564. https://doi.org/10.1038/srep14564

Ketabi, N., de Boer, T., Karakaya, M., Zhu, J., Podila, R., Rao, A. M., Kurmaev, E. Z., & Moewes, A. (2016). Tuning the electronic structure of graphene through nitrogen doping: experiment and theory. *RSC Advances*, *6*(61), 56721–56727. https://doi.org/10.1039/C6RA07546K

Krishna, R., Wade, J., Jones, A. N., Lasithiotakis, M., Mummery, P. M., & Marsden, B. J. (2017). An understanding of lattice strain, defects and disorder in nuclear graphite. *Carbon*, *124*, 314–333. https://doi.org/10.1016/j.carbon.2017.08.070

Li, Y., Wang, G., Wei, T., Fan, Z., & Yan, P. (2016). Nitrogen and sulfur co-doped porous carbon nanosheets derived from willow catkin for supercapacitors. *Nano Energy*, *19*, 165–175. https://doi.org/10.1016/j.nanoen.2015.10.038

Lu, Z., Li, S., Liu, C., He, C., Yang, X., Ma, D., Xu, G., & Yang, Z. (2017). Sulfur doped graphene as a promising metal-free electrocatalyst for oxygen reduction reaction: a DFT-D study. *RSC Advances*, *7*(33), 20398–20405. https://doi.org/10.1039/C7RA00632B

Momma, K., & Izumi, F. (2008). VESTA : a three-dimensional visualization system for electronic and structural analysis. *Journal of Applied Crystallography*, *41*(3), 653–658. https://doi.org/10.1107/S0021889808012016

Olsson, E., Chai, G., Dove, M., & Cai, Q. (2019). Adsorption and migration of alkali metals (Li, Na, and K) on pristine and defective graphene surfaces. *Nanoscale*, *11*(12), 5274–5284. https://doi.org/10.1039/C8NR10383F

Pašti, I. A., Jovanović, A., Dobrota, A. S., Mentus, S. V., Johansson, B., & Skorodumova, N. V. (2018). Atomic adsorption on graphene with a single vacancy: systematic DFT study through the periodic table of elements. *Physical Chemistry Chemical Physics*, *20*(2), 858–865. https://doi.org/10.1039/C7CP07542A

Persson, K. (2014). *Materials Data on C (SG:194) by Materials Project*. https://doi.org/10.17188/1208406

Phillips, R., Jolley, K., Zhou, Y., & Smith, R. (2021). Influence of temperature and point defects on the X-ray diffraction pattern of graphite. *Carbon Trends*, *5*, 100124. https://doi.org/10.1016/j.cartre.2021.100124

Poh, C.-K., & Shieh, H.-P. D. (2016). Density Functional Based Tight Binding (DFTB) Study on the Thermal Evolution of Amorphous Carbon. *Graphene*, *05*(02), 51–54. https://doi.org/10.4236/graphene.2016.52006

Pulido, A., Boronat, M., & Corma, A. (2011). Theoretical investigation of gold clusters supported on graphene sheets. *New Journal of Chemistry*, *35*(10), 2153. https://doi.org/10.1039/c1nj20215d

Rivera, L. M., Fajardo, S., Arévalo, M. del C., García, G., & Pastor, E. (2017). S- and N-Doped Graphene Nanomaterials for the Oxygen Reduction Reaction. *Catalysts*, *7*(9), 278. https://doi.org/10.3390/catal7090278

Rodrigo, L., Pou, P., & Pérez, R. (2016). Graphene monovacancies: Electronic and mechanical properties from large scale ab initio simulations. *Carbon*, *103*, 200–208. https://doi.org/10.1016/j.carbon.2016.02.064

Selli, D., Fazio, G., & Di Valentin, C. (2017). Modelling realistic TiO 2 nanospheres: A benchmark study of SCC-DFTB against hybrid DFT. *The Journal of Chemical Physics*, *147*(16),

164701. https://doi.org/10.1063/1.4994165

Sengupta, S., Murmu, M., Murmu, N. C., & Banerjee, P. (2021). Adsorption of redox-active Schiff bases and corrosion inhibiting property for mild steel in 1 molL−1 H2SO4: Experimental analysis supported by ab initio DFT, DFTB and molecular dynamics simulation approach. *Journal of Molecular Liquids*, *326*, 115215. https://doi.org/10.1016/j.molliq.2020.115215

Shanmugam, S., Nachimuthu, S., & Subramaniam, V. (2020). DFT study of adsorption of ions on doped and defective graphene. *Materials Today Communications*, *22*, 100714. https://doi.org/10.1016/j.mtcomm.2019.100714

Sheka, E. F., Natkaniec, I., Mel'nikov, V., & Druzbicki, K. (2015). Neutron scattering from graphene oxide paper and thermally exfoliated reduced graphene oxide. *Nanosystems: Physics, Chemistry, Mathematics*, 378–393. https://doi.org/10.17586/2220-8054-2015-6-3-378-393

Spiegelman, F., Tarrat, N., Cuny, J., Dontot, L., Posenitskiy, E., Martí, C., Simon, A., & Rapacioli, M. (2020). Density-functional tight-binding: basic concepts and applications to molecules and clusters. *Advances in Physics: X*, *5*(1), 1710252. https://doi.org/10.1080/23746149.2019.1710252

Su, Y., Zhang, Y., Zhuang, X., Li, S., Wu, D., Zhang, F., & Feng, X. (2013). Low-temperature synthesis of nitrogen/sulfur co-doped three-dimensional graphene frameworks as efficient metal-free electrocatalyst for oxygen reduction reaction. *Carbon*, *62*, 296–301. https://doi.org/10.1016/j.carbon.2013.05.067

Ugeda, M. M., Brihuega, I., Hiebel, F., Mallet, P., Veuillen, J.-Y., Gómez-Rodríguez, J. M., & Ynduráin, F. (2012). Electronic and structural characterization of divacancies in irradiated graphene. *Physical Review B*, *85*(12), 121402. https://doi.org/10.1103/PhysRevB.85.121402

Wang, J., Ma, F., & Sun, M. (2017). Graphene, hexagonal boron nitride, and their heterostructures: properties and applications. *RSC Advances*, *7*(27), 16801–16822. https://doi.org/10.1039/C7RA00260B

Warner, J. H., Lee, G.-D., He, K., Robertson, A. W., Yoon, E., & Kirkland, A. I. (2013). Bond Length and Charge Density Variations within Extended Arm Chair Defects in Graphene. *ACS Nano*, *7*(11), 9860–9866. https://doi.org/10.1021/nn403517m

Yang, M., Wang, L., Li, M., Hou, T., & Li, Y. (2015). Structural stability and O 2 dissociation on nitrogen-doped graphene with transition metal atoms embedded: A first-principles study. *AIP Advances*, *5*(6), 067136. https://doi.org/10.1063/1.4922841

Yang, Z., Nie, H., Chen, X., Chen, X., & Huang, S. (2013). Recent progress in doped carbon nanomaterials as effective cathode catalysts for fuel cell oxygen reduction reaction. *Journal of Power Sources*, *236*, 238–249. https://doi.org/10.1016/j.jpowsour.2013.02.057

Yin, L. J., Wang, W. X., Feng, K. K., Dou, R.-F., & Nie, J.-C. (2014). *The Tip-Induced Twisted Bilayer Graphene Superlattice on HOPG: Capillary Attraction Effect*. https://doi.org/10.48550/arXiv.1405.0797

Yu, Y.-X. (2013). Can all nitrogen-doped defects improve the performance of graphene anode materials for lithium-ion batteries? *Physical Chemistry Chemical Physics*, *15*(39), 16819. https://doi.org/10.1039/c3cp51689j

Zhang, Q., Khetan, A., & Er, S. (2020). Comparison of computational chemistry methods for the discovery of quinone-based electroactive compounds for energy storage. *Scientific Reports*, *10*(1), 22149. https://doi.org/10.1038/s41598-020-79153-w

Zhang, W., Kim, M., Cheng, R., Lu, W.-C., Zhang, H.-X., Ho, K. M., & Wang, C. Z. (2020). Defect Interaction and Deformation in Graphene. *The Journal of Physical Chemistry C*, *124*(4), 2370–2378. https://doi.org/10.1021/acs.jpcc.9b10622

Zhu, C., & Dong, S. (2013). Recent progress in graphene-based nanomaterials as advanced electrocatalysts towards oxygen reduction reaction. *Nanoscale*, *5*(5), 1753. https://doi.org/10.1039/c2nr33839d